Relationship between wave aberrations and histological features in *ex vivo* porcine crystalline lenses

Eva Acosta
Universidad de Santiago de Compostela
Facultad de Física
Área de Óptica
15782 Santiago de Compostela, Spain

Juan M. Bueno
Christina Schwarz
Pablo Artal
Universidad de Murcia
Centro de Investigación en Óptica y Nanofísica
Laboratorio de Óptica
Campus de Espinardo
30071 Murcia, Spain

Abstract. Wave aberrations of isolated *ex vivo* porcine crystalline lenses were measured by using a point-diffraction interferometer. This method allowed us to gain greater insight into the detailed aberration structure of eye lenses showing systematic presence of some dominant aberrations. In order of significance, astigmatism together with spherical aberration, coma, and trefoil are the main aberrations present in all lenses. We found a high correlation between the axis of both astigmatism and trefoil with the Y-shaped suture planes of the lens, revealing a subtle relationship between the induced aberrations and the histological features. © *2010 Society of Photo-Optical Instrumentation Engineers.* [DOI: 10.1117/1.3484259]

Keywords: vision; aberrations; interferometry.

The optical properties of the isolated crystalline lens determine its precise role in ocular optics. Both *in vivo* and *in vitro* methods have been previously reported to analyze this contribution. In the former, corneal aberrations were subtracted from the total ocular aberrations, assuming that the lens is mainly responsible for the remaining optics.[1–3] *In vitro* measurements of the lens were obtained using ray-tracing or Hartmann-Shack sensor approaches.[4,5] Another alternative is the use of point-diffraction interferometry (PDI)[6,7] to measure the aberrations of isolated lenses. This technique has been proven to precisely provide the details of the aberrations of lenses within an accuracy of about $\lambda/10$ and to quantify the so-called biological noise resulting from small misalignments and clusters of crystalline fiber layers throughout the entire lens.[8]

The relationship between the isolated contribution of lens surfaces and the refractive index gradient is well quantified.[9–11] Optical properties (such as defocus and spherical aberration) related to the radial symmetry of the eye lens are relatively well known; however, astigmatism and higher order aberrations are neither accurately determined nor related with the histological features of the lens. In particular, the study of lens aberrations in different animal models will complete the understanding of the optical properties of each eye.

In this paper, we use a point-diffraction interferometer (PDI) to accurately determine the wave aberration of isolated porcine lenses in order to establish correlations between histological aspects in the lens—mainly, the contribution of sutures—and their optical aberrations. The PDI has a common-path configuration,[6] offering high stability with respect to disturbing environmental noise. Its main advantage lies in its simple configuration, since it does not require a separate reference beam. Moreover, it displays the wavefront aberration directly in the fringe pattern. The PDI principle is simple: a pinhole in a semitransparent plate allows one to generate a spherical reference wavefront almost collinear to the distorted but converging wavefront. The interference taking place behind the plate produces an interference fringe pattern containing the information about the aberrated wavefront to be measured.

Because the method permits the direct visualization of constant-phase fringes, a simple visual comparison of the recorded interferogram with the simulated one with the retrieved fit coefficients allow us to[8]:

1. Choose the minimum number of Zernike polynomials that not only minimize the root mean square (rms) error of the phase differences but also can reasonably extrapolate values to regions where data could not be taken (due, for instance, to lack of visibility of fringes).

2. Choose the number and position of experimental points in order to properly reproduce desired details of the fringes.

Ex vivo porcine lenses were measured with a custom-built PDI. The experimental setup is shown in Fig. 1. Lenses were illuminated through their anterior face with a monochromatic plane wave ($\lambda=0.671$ μm), and the pinhole was placed in the vicinity of the crystalline lens focus. A 7-μm diameter pinhole was etched in a chromium oxide–coated plate with 2.3 optical density. The resulting interference pattern at the measurement plane Σ is equivalent to the interference between the converging wave exiting the eye lens and a spherical reference wave generated by diffraction at the pinhole. Thus, the interference pattern can be easily interpreted as the lens aberration plus some small amount of defocus (circular carrier fringes) and tilt (linear carrier fringes) if the pinhole is not placed precisely at the lens focus. Two examples of interferograms obtained from the same lens with different amounts of added defocus are shown in Fig. 2.

Address all correspondence to: Eva Acosta, Universidad de Santiago de Compostela, Facultad de Física, Área de Óptica, 15782, Santiago de Compostela, Spain. Tel: 34-981-563-100; E-mail: eva.acosta@usc.es
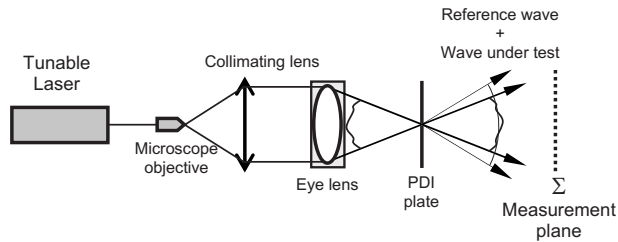
Fig. 1 Experimental setup.

Twelve crystalline lenses from 6-month-old pigs were obtained from a local abattoir. All pigs had the same genetic makeup and were fathered by the same male. All lenses presented approximately the same diameter $(9.0 \pm 0.3 \text{ mm})$ and thickness $(7.1 \pm 0.3 \text{ mm})$. The crystalline lenses were analyzed within 1 to 8 h post-mortem and were kept inside the eye globe at room temperature until the optical measurements were collected. Excised lenses were placed in a cell with planoparallel faces filled with BSS Plus intraocular irrigating solution and centered over a 5.0-mm-diam diaphragm. Porcine lenses show two sets of suture planes at each equatorial half of the lens: one Y-shaped set and another also Y-shaped but rotated 60 deg (Ref. 12). This helped us to measure the lenses under the same alignment conditions: interferograms were taken when the image of the two Y-plane suture edges intersected at only one point.

Experimental data were obtained by semiautomatic tracking of dark fringes (the nulls), as illustrated in Fig. 3, and a detailed description of the process can be found elsewhere.[8] In short, the curves obtained for each fringe represent an isophase region at the observation plane. Two consecutive curves are separated by one wavelength. A direct fit to a linear combination of Zernike polynomials is achieved with the (x,y) values of the pixels over the tracked curves and their corresponding integer number representing the phase value. It must be noted that only a selected linear combination of Zernike polynomials was chosen to fit the phase. In particular, only Zernike polynomials, Z_n^m, such that the sum of the radial and azimuthal indexes $(n,|m|)$ are equal to or less than 8 were used for the fit. We also found in all cases that $Z_4^{\pm 4}$ was not significantly present in the fit, and therefore, it was not used for the fit. As demonstrated in Ref. 8, this choice of Zernike polynomial yields the best fit in the sense that
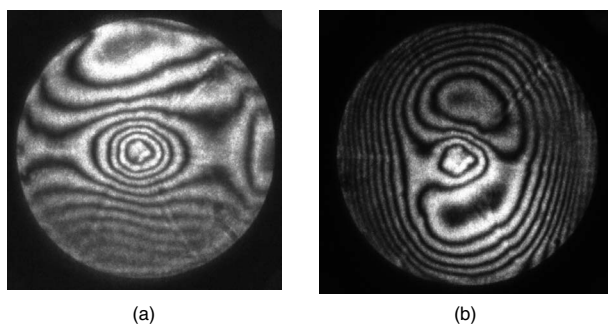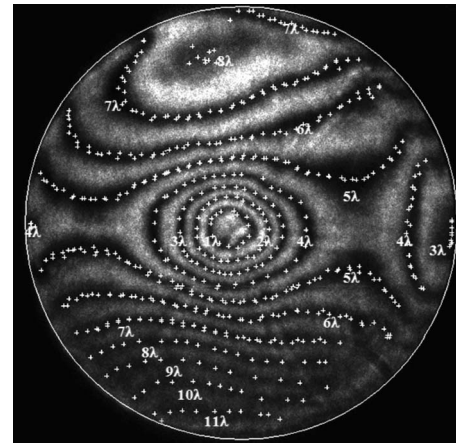

Fig. 3 Tracking of dark fringes.

1. There is maximum resemblance between the experimental and simulated with fit function interferogram.
2. The rms difference between the experimental and retrieved phases reaches a minimum value within the biological noise limits. Increasing the number of Zernike polynomials results only in fitting noise that results in a dramatic loss of the robustness of the fit coefficients.
3. Peak-to-valley (P-V) values of the difference between the experimental and theoretical phases are the smallest.

By fitting in this way, we could find that the values of the set of fitted coefficients fall within a rather narrow margin about the mean value. Figure 4 shows the average P-V absolute values expressed in wavelengths for the aberrations associated with each individual Zernike polynomial and the corresponding standard deviation. As it was not possible to precisely position all the lenses within the suture planes in the same orientation, for nonrotational aberrations we evaluated the value of the squared modulus of the $+m$ and $-m$ terms. We found primary astigmatism to be the dominant aberration, followed by spherical aberrations (both fourth and sixth order). The contribution of the trefoil terms was small although significant. The higher values of trefoil were found in the lenses that were measured after 6 to 8 h post-mortem. In order to evaluate the influence of the aberrations, we simulated interferograms with all the fitted coefficients, excluding tilts and defocus, which in some cases were induced by different positions of the pinhole to record interferograms with good contrast. Examples of these results for different lenses are
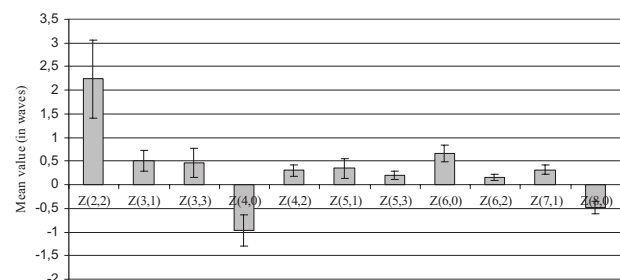

Fig. 2 (a) Interferogram in focus (pinhole close to circle of least confusion). (b) Interferogram with some amount of defocus.

Fig. 4 Mean P-V value of the Zernike coefficients and corresponding standard deviation (in wavelengths).
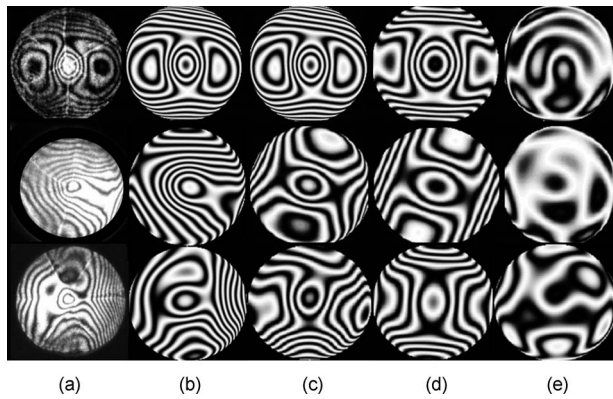
Fig. 5 In columns: (a) Recorded interferograms for three different lenses. (b) Simulated interferograms with fit coefficients. (c) Simulated interferograms with fit coefficients excluding tilts and defocus. (d) Simulated interferograms with fit coefficients only for Zernike polynomials Z_4^0, $Z_2^{\pm 2}$ and Z_6^0. (e) Interferograms for differences between (3) and (4).

Fig. 6 In columns: (a) Interferograms for three different eyes for pinhole placed very close to circle of least confusion. (b) Photographs of the corresponding edges of planes of sutures. (c) Simulated interferograms of the primary astigmatism obtained by fit coefficients. Dotted lines represent the direction of one of the focal lines.

shown in Fig. 5. Similar results were found in all the tested lenses. The first column shows the interferograms used for the fits, the second shows the interferograms reconstructed from fit, and the third shows the reconstructed interferogram without tilts and defocus. The fourth column shows the reconstructed interferograms using only the terms Z_4^0, $Z_2^{\pm 2}$, and Z_6^0; and the last column shows the difference between the interferograms of the third and the fourth columns, respectively. From these figures, it can be observed that the contributions of the coma, trefoil, and high-order astigmatism are smaller than 2 to 3 wavelengths P-V.

Also, the edges of the suture planes can be seen in the recorded interferograms, especially the first one, and a close look at the third column shows a certain correlation between the axis of the astigmatism (orientation of one of the focal lines) and one of the suture planes.

Figure 6 shows three interferograms (first column) recorded with the pinhole close to the circle of least confusion (i.e., Z_2^0 and $Z_1^{\pm 1}$ nearly zero), and the corresponding image of the edges of the suture planes (second column). In the third column, the simulated interferograms reconstructed only with the primary astigmatism are presented (with the lines representing the direction corresponding to one focal line). The axis of astigmatism and the line defining the edge of one of the suture planes are close to one another. To obtain a quantitative estimate of this result, about 50 points were manually tracked along the image of the suture edge and were fitted to a straight line, and its slope (in degrees) was compared to the slope measured on the astigmatism axis. Figure 7 shows the differences between these two angles, $\Delta\alpha$, for each measured lens. The mean value for $\Delta\alpha$ is −1 deg with a standard deviation of 7 deg, which is smaller than the angular separation between the suture plane angles (30 deg). This suggests that the astigmatism axis naturally follows the suture plane. Hence, we could conclude either that the way crystalline fibers are inserted in the suture planes depends on their orientation or that the two planes may differ slightly from the others.
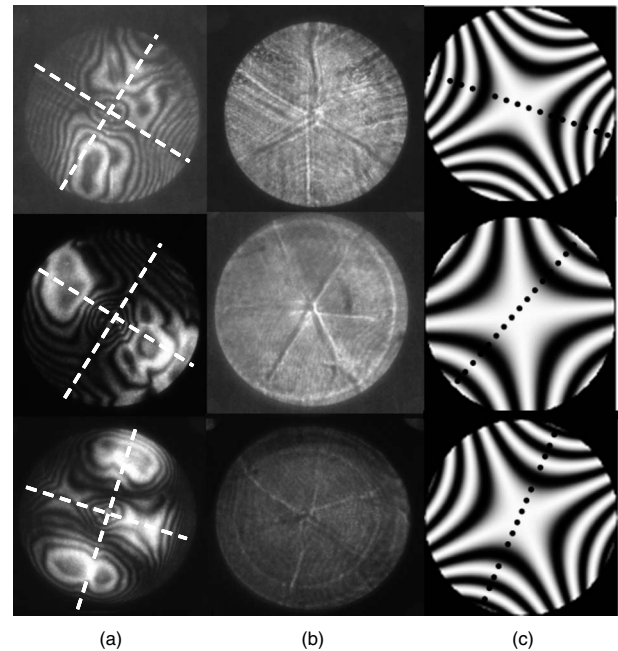
In summary, the crystalline lenses of genetically similar pigs bred under the same conditions showed a systematic presence of a similar type of optical aberrations. The most remarkable one is that the primary astigmatism is the dominant aberration, with its axis is oriented within that of the suture planes. Although in the *in vitro* experiment, it was not possible to distinguish which of the sutures was responsible for the astigmatism, there is no reason to believe that the axis of astigmatism could randomly switch from one suture plane to another, and therefore, we are inclined to conclude that the same suture plane leads to a focal line aligned with it. The next most significant aberrations are fourth- and sixth-order spherical aberrations, although it must be considered that the excised lenses were fully accommodated and resting on the
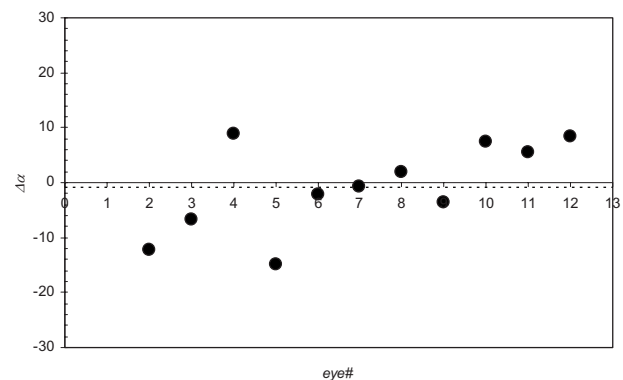

Fig. 7 Difference between angle of axis of astigmatism and angle of suture planes for each measured eye. Dotted line represents mean value of the differences.

cell floor. The other terms accounted for less than 2λ P-V of the total aberration, but they were statistically significant in the fits. The contribution of aberrations with an azimuthal frequency of 3 is quite small, and 4 is not significant in the fits. We found that the amount of trefoil increased mainly in those eyes measured more than 6 h post-mortem; hence, it can be concluded that the presence of trefoil may be related with some degenerative process of the lens beginning in the suture planes. Although from this study, we can not yet relate the significant presence of coma (lower and higher orders) with the suture planes structure or any other histological feature, we could say that the presence of the same pattern of nonsymmetric aberrations of azimuthal order 2 and 3 as well as the absence of order 4 or higher may indicate that there could be an aberration control mechanism in the growing process of the lens. These results obtained *ex vivo* could be further incorporated in eye modeling to better understand the suggested coupling of the corneal and lenticular aberrations.

Acknowledgments

References

1. P. Artal and A. Guirao, "Contributions of the cornea and the lens to the aberrations of the human eye," *Opt. Lett.* **23**, 1713–1715 (1998).
2. P. Artal, A. Guirao, E. Berrio, and D. R. Williams, "Compensation of corneal aberrations by the internal optics in the human eye," *J. Vision* **1**, 1–8 (2001).
3. M. Millodot and J. Sivak, "Contribution of the cornea and lens to the spherical aberration of the eye," *Vision Res.* **19**, 685–687 (1979).
4. J. G. Sivak and R. O. Kreuzer, "Spherical aberration of the crystalline lens," *Vision Res.* **23**, 59–70 (1983).
5. A. Roorda and A. Glasser, "Wave aberrations of the isolated crystalline lens," *J. Vision* **4**, 250–261 (2004).
6. C. Koliopoulos, O. Kwon, R. Shagam, J. C. Wyant, and C. R. Hayslett, "Infrared point diffraction interferometer," *Opt. Lett.* **3**, 118–120 (1978).
7. J. M. Bueno, E. Acosta, C. Schwarz, and P. Artal, "Wavefront measurements of phase plates combining a point-diffraction interferometer and a Hartmann-Shack sensor," *Appl. Opt.* **49**, 450–456 (2010).
8. E. Acosta, D. Vazquez, and L. Rodriguez-Castillo, "Analysis of the optical properties of crystalline lenses by point diffraction interferometry," *Ophthalmic Physiol. Opt.* **29**, 235–246 (2009).
9. D. Borja, F. Manns, A. Ho, N. Ziebarth, A. M. Rosen, R. Jain, A. Amelinckx, E. Arrieta, R. C. Augusteyn, and J. M. Parel, "Optical power of the isolated human crystalline lens," *Invest. Ophthalmol. Visual Sci.* **49**, 2541–2548 (2008).
10. J. M. Bueno, C. Schwarz, E. Acosta, and P. Artal, "Surfaces geometry and optical aberrations of *ex vivo* crystalline lenses," *Proc. SPIE* **7550**, 75502D (2010).
11. M. C. W. Campbell, "Contributions to the optical quality of the eye: implications for 'perfect' optical correction," in *Vision Science and Its Applications*, OSA Technical Digest, Optical Society of America, Washington, DC (2000).
12. J. R. Kuszak, R. K. Zoltoski, and C. E. Tiedemann, "Development of lens sutures," *Int. J. Dev. Biol.* **48**, 889–902 (2004).